Anomalous Nernst effect in epitaxial graphene modulated by external fields

Xiaogang Zhang [●],[1] Yafang Xu,[2,*] and Guojun Jin[1,3,†]

[1]*School of Physics Science and Technology, Kunming University, Kunming 650214, China*
[2]*College of Physics Science and Technology, Yangzhou University, Yangzhou 225002, China*
[3]*National Laboratory of Solid State Microstructures, Department of Physics, and Collaborative Innovation Center of Advanced Microstructures, Nanjing University, Nanjing 210093, China*

Under the coaction of off-resonant circularly polarized light and antiferromagnetic exchange field, epitaxial graphene undergoes various topological phases. Considering the self-rotation of the wave packet and the Berry curvature driving topological effect, we investigate the spin- and valley-dependent anomalous Nernst effect in epitaxial graphene and propose two alternative methods to differentiate various topological phases. Firstly, the charge Nernst current appears only when the light field exists, while for achieving the spin Nernst current, two external fields must be applied simultaneously. Due to the existence of a substrate potential, a thermally induced pure valley current can be demonstrated, and its magnitude and sign can be controlled by changing the antiferromagnetic exchange field. Single-spin and single-valley Nernst currents can be collected in the quantum valley Hall–quantum anomalous Hall insulator phase. Secondly, the abundant topological phases in epitaxial graphene can be distinguished by detecting the sign change of the charge, spin, and valley Nernst conductivities by tuning the Fermi level. Thirdly, the temperature dependence provides another efficient method to distinguish various topological phases. After deriving an analytical expression from the semiclassical Mott relation, it is shown that by adjusting the sample temperature, the variation trend of the spin-valley Nernst currents can be detected. These findings are experimentally verifiable in the future and can be promising for spin and valley caloritronic applications.

I. INTRODUCTION

Since Novoselov and Geim *et al.* creatively used the mechanical exfoliation method to successfully prepare stable graphene in 2004, graphene has rapidly become one of the hottest research subjects in the fields of condensed-matter physics and materials science [1,2]. A graphene monolayer is a two-dimensional hexagonal honeycomb crystal. Due to the simplicity of the lattice structure, the controllability of the external fields, and the potential value in theory and application, researchers have been inspired to study the novel physical properties of graphene, such as its electrical, thermal, optical, mechanical, magnetic, and topological properties [3–7]. This has also stimulated research on other single-layered materials such as silicene, germanene, molybdenum disulfide, etc. In momentum space, graphene has two degenerate but inequivalent valleys at the corners of the first Brillouin zone. Due to the large distance between the two valleys, intervalley scattering is suppressed strongly [8,9]. Similar to the spin degree of freedom, valley degree of freedom is known as pseudospins. Based on it, a new discipline, namely, valleytronics, is also a hot research topic now [10].

Compared with a large amount of research on the electrical transport properties of graphene, thermoelectric transport has more potential applications in thermal energy-saving and dissipation devices, especially regarding the spin- and valley-dependent anomalous Nernst effect. The anomalous Nernst effect describes a transverse current induced by a longitudinal temperature gradient in the presence of Berry curvature [11]. Under the modulation of an off-resonant light and a substrate potential, the valley-polarized Nernst effect has been researched [12]. However, under the coaction of the off-resonant light and antiferromagnetic fields, which break the time-reversal, spatial inversion, and spin-rotation symmetries, the spin- and valley-dependent anomalous Nernst effect and the correspondence between various topological phases and transport properties have not been fully investigated and explored in epitaxial graphene. Based on these reasons, we investigate the spin- and valley-dependent anomalous Nernst effect under the modulation of external fields. The results indicate that the charge Nernst current is observed exclusively in the presence of a light field. The generation of spin Nernst current requires the simultaneous application of two external fields. Furthermore, a fundamental objective of valleytronics is to generate and detect controllable pure valley currents. The presence of the substrate potential enables the demonstration of thermally induced pure valley currents whose magnitude and sign can be controlled by adjusting the antiferromagnetic exchange field.

Under the modulation of the off-resonant light and antiferromagnetic exchange field, epitaxial graphene undergoes a sequentially quantum valley Hall insulator (QVHI) phase,

_____
*Corresponding author: yfxu@yzu.edu.cn
†Corresponding author: gjin@nju.edu.cn

quantum anomalous Hall insulator (QAHI) phase, quantum spin valley Hall insulator (QSVHI) phase, and QVH-QAHI phase [13]. In principle, experimentally detecting whether a material is a topological insulator can be judged by observing the edge states of nanoribbons or by measuring the quantized Hall conductivity. Some special methods can also be used to distinguish different topological insulator phases. For example, Ezawa has proposed that diamagnetism or optical circular dichroism can be exploited to distinguish band insulator and topological insulator phases in silicene [14,15]. For more complex phase transitions, the discrimination methods are relatively few. Here, based on the anomalous Nernst effect associated with Berry curvature [12,16–21], we find an alternative method to characterize the abundant topological phases by detecting the sign change of the charge, spin, and valley Nernst conductivities by tuning the Fermi level.

Furthermore, the anomalous Nernst conductivity is determined not only by the Berry curvature but also by the entropy density around the Fermi level. In order to study the thermoelectric transport properties clearly, we consider their temperature dependence. It can be found that the sign change of the Nernst conductivity is robust against a weak temperature. The magnitudes of the valley Nernst conductivity in the QVHI phase, the charge Nernst conductivity in the QAHI phase, and the spin Nernst conductivity in the QVH-QAHI phase are enhanced significantly as the temperature increases. We give an analytical expression for the spin-valley-dependent Nernst conductivity at low temperatures, and the validity of the semiclassical Mott relation is verified in a certain temperature range. Importantly, we propose another alternative method to characterize whether a topological phase transition occurs by probing the changes in spin-valley-dependent Nernst currents under the adjustment of the sample temperature.

In this work we build a theoretical framework to populate the valleys and spins under the competition between the staggered sublattice potential, off-resonant light, and antiferromagnetic exchange field in graphene and give the correspondence between various topological phases and Nernst conductivity by tuning the Fermi level or temperature. In fact, it has been investigated that the materials MnPS$_3$ and MnPSe$_3$ are native antiferromagnets, which have similar low-energy effective Hamiltonians [22]. Why not consider the materials MnPS$_3$ and MnPSe$_3$ as our research object? On one hand, the antiferromagnetism in these materials is just a theoretical result, and on the other hand, the topological phase transition has not been very clear in these finite-sized materials due to complicated hopping energies. On account of its tunability and simplicity, graphene is more suitable as our subject of study. In addition, the focus of the previous research in Ref. [13] is concentrated on discovering new topological phases such as topological metal and half-metal phases. However, here we propose two alternative methods to differentiate various topological phases by tuning the Fermi level or temperature. It provides a new visual angle for detecting the various topological phases and is a deeper research than the previous work.

The outline of the paper is as follows. In Sec. II, the theoretical model and basic formalism are constructed and derived. In Sec. III we investigate the spin- and valley-related anomalous
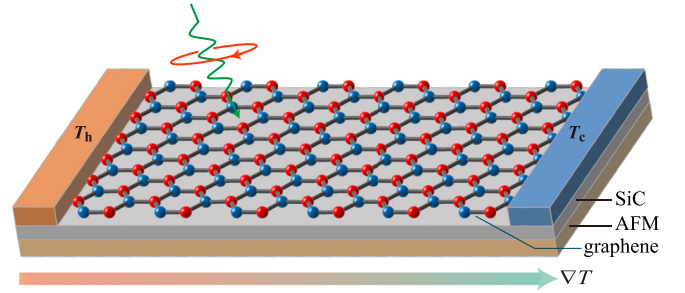
FIG. 1. Schematic of a graphene monolayer, which is irradiated by an off-resonant circularly polarized light and epitaxially grown on a SiC substrate. The antiferromagnetic field can be achieved by the proximity effect from an antiferromagnet. The temperature gradient ∇T is applied in the longitudinal direction.

Nernst effect in epitaxial graphene under the modulation of external fields. In Sec. IV an executable method to characterize the abundant topological phases by tuning the Fermi level to detect the sign change of the charge, spin, and valley Nernst conductivities is given. In Sec. V we consider the influence of temperature on the anomalous Nernst effect and propose another effective method to distinguish topological phases by adjusting the sample temperature. Finally, a summary is given in Sec. VI.

II. MODEL AND FORMULATION

The model is shown in Fig. 1, where a temperature gradient is applied between the hot and cold electrodes, a graphene monolayer, subjected to off-resonant circularly polarized light and an antiferromagnetic field, is epitaxially grown on a SiC substrate. In the low-energy approximation, the Hamiltonian of the system can be written as

$$\mathcal{H} = \hbar v_F(\eta \tau_x k_x + \tau_y k_y) + \lambda_z \tau_z + \eta \lambda_\omega \tau_z + \lambda_{AF} \sigma_z \tau_z, \quad (1)$$

where $\eta = +(-)$ represents the valley K (K'), σ_z and $\tau_{x,y,z}$ are Pauli matrices of the spin and the sublattice pseudospin, respectively. The first term is the Dirac Hamiltonian arisen from the nearest-neighbor hopping energy, $v_F = \sqrt{3}at/2\hbar \simeq 10^6$ m/s is the Fermi velocity with the lattice constant $a = 2.46$ Å, and the nearest-neighbor hopping integral $t = 2.97$ eV. The second term is the staggered sublattice potential induced by the SiC substrate, which breaks the spatial inversion symmetry. When graphene is epitaxially grown on a SiC substrate, in the experiment, the energy gap λ_z can reach several meV to 0.26 eV [23,24]. The third term is the Haldane term induced by the off-resonant circularly polarized light [12,13,25]. The illumination parameter $\lambda_\omega = 8\pi\alpha\xi I v_F^2/\omega^3$, with $\alpha \simeq 1/137$ as the fine-structure constant, I as the laser intensity, ω as the light frequency, and $\xi = +(-)$ as the right (left) circulation of light. For the off-resonant light, it does not directly excite electrons but effectively changes the energy band structure through photon absorption and emission processes [26]. Its photon energy needs to be much higher than the bandwidth of graphene, which requires that off-resonant light should satisfy $\hbar\omega \gg t$, i.e., the frequency is not less than 3500 THz. We adopt the lowest frequency of about 3500 THz, so when the range of laser intensity is from 10^{10} to 1.5×10^{12} W/cm^2,

the illumination parameter $|\lambda_\omega|$ can range from 0.0026 to 0.39 eV [27]. The last term is the antiferromagnetic exchange term [28,29]. For the antiferromagnetic exchange field, it was proposed theoretically [30] that a honeycomb lattice antiferromagnet can be attached to the graphene monolayer to produce an antiferromagnetic field by the proximity effect. Recently, more first-principles calculations show that the layered antiferromagnetic semiconductor $MnPSe_3$ is a good candidate [22], which can serve as the substrate of graphene and induce an antiferromagnetic exchange field [31,32]. The antiferromagnetic field can be tuned by changing the interlayer distance between graphene and $MnPSe_3$. In the experiment, proximity-induced ferromagnetism in graphene has been demonstrated [33], and antiferromagnetic exchange coupling can be realized between two ferromagnets mediated by a layer of graphene [34]. Although the proximity-induced antiferromagnetic exchange field has not been observed in our experiment at present, the proposed theoretical model is expected to be possible in the future with the advanced experimental techniques.

Solving the Schrödinger equation for $\mathcal{H}$, we can obtain the dispersion related to the spin and valley, which is written as

$$E^n_{\eta,s_z}(k) = n\sqrt{(\hbar v_F k)^2 + \Delta^2_{\eta,s_z}}, \tag{2}$$

where $n = +(-)$ represents the conduction (valence) band, $s_z = +(-)$ denotes the spin-up (down), $k = \sqrt{k_x^2 + k_y^2}$ is the modulus of wave vector $\boldsymbol{k}$, and $\Delta_{\eta,s_z} = \lambda_z + \eta\lambda_\omega + s_z\lambda_{AF}$ is equivalent to an effective mass. We can fully control the effective mass of each spin and valley independently, enabling spin-valley electronics in graphene. By solving the eigenstates and using the definition of Berry curvature $\boldsymbol{\Omega}_n(\boldsymbol{k}) = \nabla \times \langle u_n(\boldsymbol{k})|i\nabla_{\boldsymbol{k}}|u_n(\boldsymbol{k})\rangle$, where $u_n(\boldsymbol{k})$ is the periodic part of the Bloch wave function of the nth Bloch band with wave vector $\boldsymbol{k}$, we obtain the analytical expression of the spin-valley-dependent Berry curvature. It is written as

$$\Omega^n_{\eta,s_z}(k) = n\eta \frac{\hbar^2 v_F^2 \Delta_{\eta,s_z}}{2\left[(\hbar v_F k)^2 + \Delta^2_{\eta,s_z}\right]^{3/2}}. \tag{3}$$

The integral of the Berry curvature over the Brillouin zone is the Chern number. The topological insulator phase can be characterized by four independent Chern numbers, i.e., the charge Chern number C_c, the spin Chern number C_s, the valley Chern number C_v, and the spin-valley Chern number C_{sv}.

If the symmetry of spatial inversion or time reversal of the system is broken, a nonzero Berry curvature will be produced. When the system has a nonzero Berry curvature, the Bloch electrons will obtain a transverse velocity perpendicular to the direction of the external electric field, i.e., $\dot{\boldsymbol{r}} = \frac{1}{\hbar}\frac{\partial E_n(\boldsymbol{k})}{\partial \boldsymbol{k}} + \frac{e}{\hbar}\mathcal{E} \times \boldsymbol{\Omega}_n(\boldsymbol{k})$, where $E_n(\boldsymbol{k})$ is the nth band energy, $\mathcal{E}$ is the external electric field, and $\boldsymbol{\Omega}_n(\boldsymbol{k})$ is the Berry curvature. The Berry curvature is equivalent to a magnetic field in the wave-vector space, and it will bring about very unique physical phenomena, such as the anomalous Nernst effect [35–37], anomalous Hall effect [38–40], etc. Considering the topological effect and the Berry curvature, the spin- and valley-dependent transverse Nernst current induced by the longitudinal temperature

gradient field can be written as

$$\boldsymbol{J}_{\eta,s_z} = -\frac{\nabla T}{T} \times \sum_n \frac{e}{\hbar}\int \frac{d\boldsymbol{k}}{(2\pi)^2}\boldsymbol{\Omega}^n_{\eta,s_z}\Big\{\big[E^n_{\eta,s_z}(k) - E_F\big]f^n_{\eta,s_z}(k)$$
$$+ k_BT\ln\big[1 + e^{-\frac{E^n_{\eta,s_z}(k)-E_F}{k_BT}}\big]\Big\}, \tag{4}$$

where $f^n_{\eta,s_z}(k) = 1/\{1 + \exp[(E^n_{\eta,s_z}(k) - E_F)/k_BT]\}$ is the Fermi distribution function for valley η, spin s_z, and band n, k_B is the Boltzmann constant, and E_F is the Fermi level. According to the definition of anomalous Nernst conductivity $J_y = N(-\nabla_x T)$, the spin-valley-dependent Nernst conductivity can be written as

$$N_{\eta,s_z} = \frac{ek_B}{\hbar}\sum_n \int \frac{d\boldsymbol{k}}{(2\pi)^2}\Omega^n_{\eta,s_z}\mathcal{S}^n_{\eta,s_z}(k), \tag{5}$$

where $\mathcal{S}^n_{\eta,s_z}(k) = -f^n_{\eta,s_z}(k)\ln f^n_{\eta,s_z}(k) - [1 - f^n_{\eta,s_z}(k)]\ln[1 - f^n_{\eta,s_z}(k)]$ is the entropy density. The entropy density has a peak at E_F. When the energy is beyond the range of $[E_F - 5k_BT, E_F + 5k_BT]$, the entropy density is basically zero. The charge, spin, and valley Nernst conductivities can then be defined as

$$N_c = \sum_{\eta,s_z} N_{\eta,s_z}, \; N_s = \sum_{\eta,s_z} s_z N_{\eta,s_z}, \; N_v = \sum_{\eta,s_z} \eta N_{\eta,s_z}. \tag{6}$$

In the experiment, the charge Nernst conductivity can be directly measured by using an amperometer, and the spin and valley Nernst currents can be measured by a Hall bar geometry through the inverse spin or valley Hall effect [41–43].

III. SPIN- AND VALLEY-RELATED ANOMALOUS NERNST EFFECT

In the numerical calculations, we set the temperature $T = 300$ K, the staggered sublattice potential $\lambda_z = 0.1$ eV, and the irradiated off-resonant light to be right circularly polarized. The unit for the Nernst conductivity is $ek_B/h \approx 3.33$ nA/K, and the energy unit (E_F, λ_ω, and λ_{AF}) is electronvolts. Before studying the property of the anomalous Nernst effect, we first discuss the characteristics of the Berry curvature of the conduction band. In Fig. 2 we chose four sets of parameters to display the Berry curvature, and the four sets of parameters were selected from different topological phases. The red solid (blue dashed) lines denote the Berry curvatures with spin-up (-down). It is observed that when there are no external fields, in the K (K') valley, the Berry curvatures with spin-up and spin-down are all positive (negative), as shown in Fig. 2(a). The Chern numbers are $(0, 0, -2, 0)$, corresponding to the QVHI phase. When a light field is applied with $\lambda_\omega = 2\lambda_z$, both the time-reversal and the sublattice pseudospin symmetries are broken. Compared with those in Fig. 2(a), the Berry curvatures in the K valley decrease, and the reversal of Berry curvature occurs in the K' valley, as shown in Fig. 2(b). The QVHI phase undergoes a topological phase transition to the QAHI phase with Chern numbers $(-2, 0, 0, 0)$. In Fig. 2(c) only the antiferromagnetic exchange field exists, and it satisfies $\lambda_{AF} = 2\lambda_z$. Compared with those in Fig. 2(a), the Berry curvatures with spin-up decrease in both the K and K' valleys, while the reversal of Berry curvature occurs with spin-down, which is in the QSVHI phase with Chern numbers
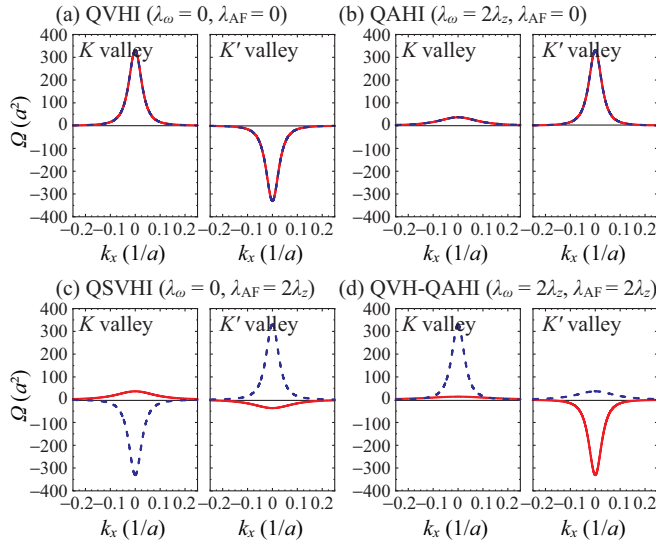
FIG. 2. Berry curvatures of the conduction-band electrons in different topological phases. The Berry curvature in the vertical axis is in units of a^2; the wave vector in the horizontal axis is in units of $1/a$. (a)–(d) Berry curvatures of the K and K' valleys. The red solid (blue dashed) line represents the Berry curvature with spin-up (-down). The staggered potential λ_z is fixed at 0.1 eV.

FIG. 3. Charge, spin, and valley Nernst conductivities as functions of the Fermi level. The parameters of external fields are chosen exactly as those in Fig. 2.

$(0, 0, 0, -2)$. When both the light field and antiferromagnetic exchange field exist with $\lambda_\omega = 2\lambda_z$ and $\lambda_{AF} = 2\lambda_z$, the external fields and staggered sublattice potential compete with each other. In the K valley, the Berry curvatures with spin-up and -down are all positive, while in the K' valley the Berry curvature with spin-up is negative but the one with spin-down is positive, as shown in Fig. 2(d). Due to the changed Berry curvatures, the Chern numbers become $(-1, 1, -1, -1)$, which correspond to the QVH-QAHI phase. Therefore we can tune the amplitude and sign of the Berry curvature by manipulating the off-resonant light and the antiferromagnetic field.

The spin-valley-dependent Nernst conductivity is calculated from Eq. (5) by integrating the Berry curvature; then the charge, spin, and valley Nernst conductivities can be obtained from Eq. (6). In Fig. 3 we plot the charge, spin, and valley Nernst conductivities as functions of the Fermi energy E_F. The parameters of the external fields correspond exactly to those in Fig. 2. When there are no external fields, due to the fact that the signs of the Berry curvatures are opposite in different valleys, satisfying $\Omega_{K,\uparrow} = \Omega_{K,\downarrow} = -\Omega_{K',\uparrow} = -\Omega_{K',\downarrow}$, the spin-valley-dependent Nernst conductivities are related by $N_{K,\uparrow} = N_{K,\downarrow} = -N_{K',\uparrow} = -N_{K',\downarrow}$. Hence, $N_c = N_s = 0$, where N_v is finite, as shown in Fig. 3(a). In Fig. 3(b) when only a light field exists, the Berry curvatures in the same valley from different spins are equal, i.e., $\Omega_{K,\uparrow} = \Omega_{K,\downarrow}$ and $\Omega_{K',\uparrow} = \Omega_{K',\downarrow}$; therefore the Nernst conductivities satisfy $N_{K,\uparrow} = N_{K,\downarrow}$ and $N_{K',\uparrow} = N_{K',\downarrow}$. Comparing with those in Fig. 3(a), the N_s is still zero, but N_c and N_v can be obtained at the same time, and the sign change of N_v occurs as E_F varies. In Fig. 3(c) when only an antiferromagnetic field exists, the Berry curvatures for the same spin but different valleys satisfy $\Omega_{K,\uparrow} = -\Omega_{K',\uparrow}$ and $\Omega_{K,\downarrow} = -\Omega_{K',\downarrow}$. Therefore the Nernst conductivities have the relations $N_{K,\uparrow} = -N_{K',\uparrow}$ and $N_{K,\downarrow} = -N_{K',\downarrow}$. In this case both the N_c and N_s are zero, and N_v is finite. In Fig. 3(d), when the
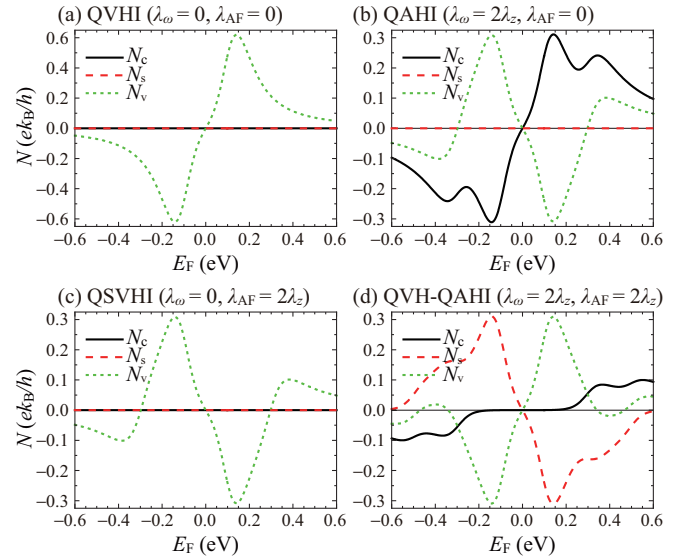
light field and the antiferromagnetic field coexist, N_c, N_s, and N_v are all nonzero. The signs of N_c and N_v are the same but are opposite to N_s. So if we want to obtain the spin Nernst current, a light field and an antiferromagnetic field must be applied simultaneously.

People may notice that the parameters used in the figure just now are only for four specific points in the phase diagram. In order to explore the possible parameter dependencies, we plot the contour plots of N_c, N_s, and N_v as functions of λ_ω and λ_{AF}, as shown in Fig. 4. It can be seen from Fig. 4(a) that the charge Nernst conductivity N_c is odd in λ_ω but even in λ_{AF}. When $\lambda_\omega = 0$ there is no charge Nernst current. In Fig. 4(b) the spin Nernst conductivity N_s is odd with respect to λ_ω and λ_{AF}, and symmetric about $\lambda_\omega = \pm\lambda_{AF}$. When $\lambda_\omega = 0$ or $\lambda_{AF} = 0$, it is zero, so to obtain spin Nernst current, two external fields must exist simultaneously. In Fig. 4(c) the valley Nernst conductivity has four symmetric axes. The value of N_v is largest at the center. The sign of the charge and spin Nernst conductivities can be changed by reversing the polarization direction of light. To clarify the relation between the symmetries of the external fields and the Nernst conductivities, we summarize the correspondences between the time-reversal symmetry (TRS), spin-rotation symmetry (SRS), and sublattice pseudospin symmetry (SPS) with the Nernst currents in Table I. From it the Nernst currents corresponding to different external fields can be seen clearly.

By using Eq. (5) we can define the spin and valley polarizations P_s and P_v: $P_s = (|N_\uparrow| - |N_\downarrow|)/(|N_\uparrow| + |N_\downarrow|)$ and $P_v = (|N_K| - |N_{K'}|)/(|N_K| + |N_{K'}|)$. $N_{s_z} = N_{K,s_z} + N_{K',s_z}$ is the current in the spin-s_z channel, while $N_\eta = N_{\eta,\uparrow} + N_{\eta,\downarrow}$ represents the current in the η valley. As shown in Fig. 5(a), when $\lambda_\omega = 0$ and $\lambda_{AF} = 0$, N_K and $N_{K'}$ flow in opposite directions and have the same magnitude, so a pure valley current N_v with no charge counterpart is generated. If we fix $E_F = 0.15$ eV and $\lambda_\omega = 0$, and adjust the antiferromagnetic field, the magnitude and direction of the pure valley current can be changed by
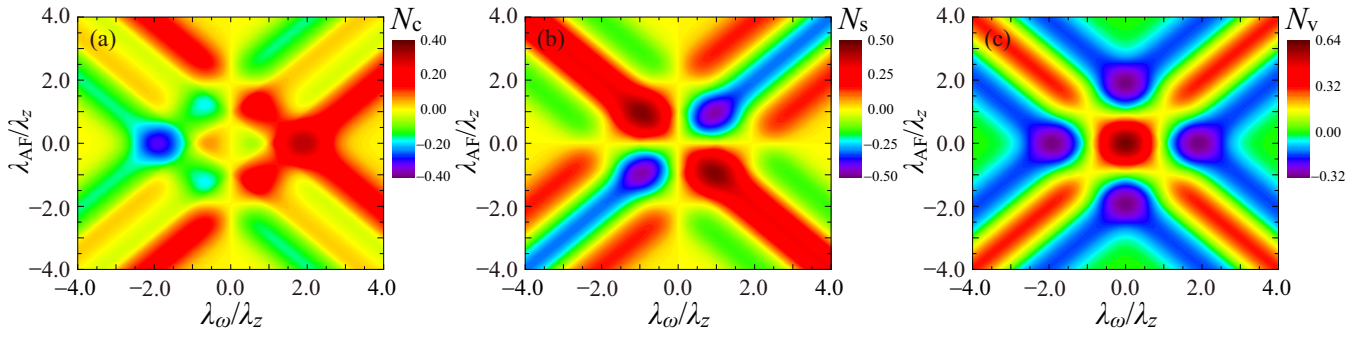
FIG. 4. Contour plots of the charge, spin, and valley Nernst conductivities as functions of λ_ω and $\lambda_{\rm AF}$ in the reduced units using $\lambda_z = 0.1$ eV. The Fermi level is set as $E_{\rm F} = 0.15$ eV.

tuning $\lambda_{\rm AF}$, as shown in Fig. 5(b). Figures 5(c) and 5(d) show the $P_{\rm s}$ and $P_{\rm v}$ as functions of λ_ω and $\lambda_{\rm AF}$, respectively. The spin polarization $P_{\rm s}$ is odd in $\lambda_{\rm AF}$ but even in λ_ω. $P_{\rm s}$ changes significantly by changing the antiferromagnetic exchange field. The valley polarization $P_{\rm v}$ is odd in λ_ω but even in $\lambda_{\rm AF}$. Similar to the spin polarization $P_{\rm s}$, the valley polarization $P_{\rm v}$ changes dramatically by changing the light field. It can also be seen that a full valley-polarized current can be achieved, and the sign of valley polarization can be changed by reversing the polarization of the light. In order to obtain a pure valley-polarized Nernst current, it is necessary to adjust the external fields to satisfy $N_{\eta,\uparrow} + N_{\eta,\downarrow} = 0$, i.e., $\Omega_{\eta,\uparrow} = -\Omega_{\eta,\downarrow}$. Through analytical analyses, the condition for generating the pure valley-polarized Nernst current is $\lambda_\omega = -\eta\lambda_z$, and the corresponding Nernst current only comes from valley $-\eta$. In addition, from Figs. 5(c) and 5(d) it can also be found that relatively high spin and valley polarizations ($\geqslant 0.90$) can be achieved in a wide parameter region for λ_ω and $\lambda_{\rm AF}$. The region where $|\lambda_\omega|$ is close to λ_z can achieve relatively high valley polarization currents.

IV. TOPOLOGICAL CORRESPONDENCE WITH ANOMALOUS NERNST CONDUCTIVITY

Under the coaction of the off-resonant light and antiferromagnetic field, epitaxial graphene undergoes various topological phases, including QVHI phase, QAHI phase,

TABLE I. The relation between symmetry of external field and Nernst conductivity. Yes (No) means to keep (break) a symmetry. $\checkmark$ ($\times$) indicates the presence (absence) of a corresponding Nernst current in the system.

External	Symmetry			Nernst conductivity		
field	TRS	SRS	SPS	$N_{\rm c}$	$N_{\rm s}$	$N_{\rm v}$
λ_z	Yes	Yes	No	$\times$	$\times$	$\checkmark$
λ_z	Yes	Yes	No	$\checkmark$	$\times$	$\checkmark$
λ_ω	No	Yes	No			
λ_z	Yes	Yes	No	$\times$	$\times$	$\checkmark$
$\lambda_{\rm AF}$	No	No	No			
λ_z	Yes	Yes	No	$\checkmark$	$\checkmark$	$\checkmark$
λ_ω	No	Yes	No			
$\lambda_{\rm AF}$	No	No	No			

QSVHI phase, and QVH-QAHI phase. To clarify the relation between various topological phases and transport properties, the relations between all topological phases and spin-valley-dependent Nernst currents are summarized in Table II. For the QVHI phase, the valley Nernst currents are separated. In the QAHI phase, all four components of the Nernst current have the same direction, achieving unidirectional spin-valley Nernst currents. For the QVH-QAHI phase, the three components of the Nernst current have the same direction and the current with one valley and one spin have opposite directions. By tuning the external fields to make graphene lie in this phase, single-valley and one-spin Nernst currents can be collected. However, in the QSVHI phase, the spin and valley Nernst currents are mixed at one end. It is difficult to distinguish it from QVHI and QVH-QAHI phases.

In principle, the most instinctive method to detect and distinguish topological phases is to observe the edge states of nanoribbons in addition to calculating the Chern numbers. Here we propose to distinguish topological phases by judging the sign change of the Nernst conductivity. In Fig. 6 we plot charge, spin, and valley Nernst conductivities as functions of
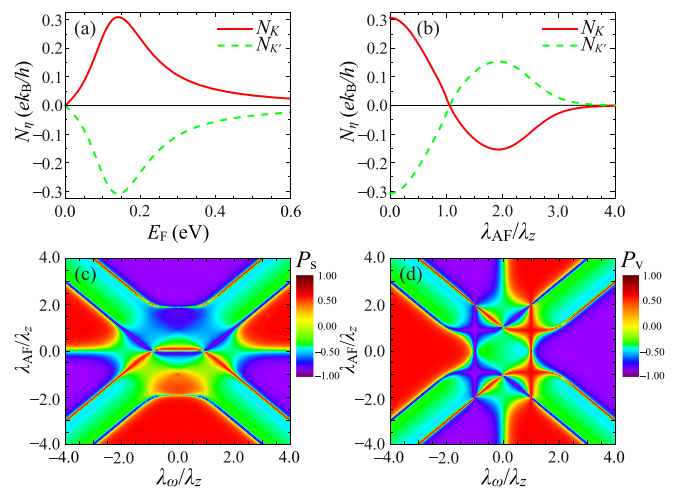
FIG. 5. (a) Valley-resolved Nernst conductivity N_η as a function of $E_{\rm F}$ with $\lambda_\omega = 0$ and $\lambda_{\rm AF} = 0$. (b) Valley-resolved Nernst conductivity N_η as a function of $\lambda_{\rm AF}$ with $E_{\rm F} = 0.15$ eV and $\lambda_\omega = 0$. (c) Spin polarization $P_{\rm s}$ and (d) valley polarization $P_{\rm v}$ as functions of λ_ω and $\lambda_{\rm AF}$. The other parameters are $E_{\rm F} = 0.15$ eV, $\lambda_z = 0.1$ eV, and $T = 300$ K.

TABLE II. The relation between all topological phases and the spin-valley Nernst conductivities. $+(-)$ represents the direction of the spin-valley Nernst current.

Topological phase	Chern numbers $[\mathcal{C}_c, \mathcal{C}_s, \mathcal{C}_v, \mathcal{C}_{sv}]$	Spin-valley Nernst conductivity			
		$N_{K,\uparrow}$	$N_{K,\downarrow}$	$N_{K',\uparrow}$	$N_{K',\downarrow}$
QVHI	$[0, 0, -2, 0]$	$+$	$+$	$-$	$-$
QAHI	$[-2, 0, 0, 0]$	$+$	$+$	$+$	$+$
	$[2, 0, 0, 0]$	$-$	$-$	$-$	$-$
QSVHI	$[0, 0, 0, -2]$	$+$	$-$	$-$	$+$
	$[0, 0, 0, 2]$	$-$	$+$	$+$	$-$
QVH-QAHI	$[-1, -1, -1, 1]$	$+$	$+$	$+$	$-$
	$[-1, 1, -1, -1]$	$+$	$+$	$-$	$+$
	$[1, -1, -1, -1]$	$+$	$-$	$-$	$-$
	$[1, 1, -1, 1]$	$-$	$+$	$-$	$-$

Fermi energy E_F. It is found that by modulating E_F in the QVHI phase ($\lambda_\omega = 0.5\lambda_z$, $\lambda_{AF} = 0.25\lambda_z$), the signs of N_c and N_s are changed while the sign of N_v is always unchanged, as shown in Fig. 6(a). In the QAHI phase ($\lambda_\omega = 1.5\lambda_z$, $\lambda_{AF} = 0.25\lambda_z$), the signs of N_v and N_s are changed while the sign of N_c always remains unchanged, as shown in Fig. 6(b). In the QSVHI phase ($\lambda_\omega = 0.5\lambda_z$, $\lambda_{AF} = 2\lambda_z$), the signs of N_c, N_v, and N_s are changed, as shown in Fig. 6(c). In addition, as shown in Fig. 6(d), in the QVH-QAHI phase ($\lambda_\omega = 1.5\lambda_z$, $\lambda_{AF} = 2\lambda_z$), the signs of N_c and N_v are changed while the sign of N_s always remains unchanged.

To explore possible parameter dependencies, the light fields λ_ω/λ_z are fixed as 0.5 and 1.5, respectively, and we calculate the charge, spin, and valley Nernst conductivities as functions of E_F and λ_{AF}, as shown in Fig. 7. The same result can be obtained in QVHI, QAHI, and QSVHI phases,
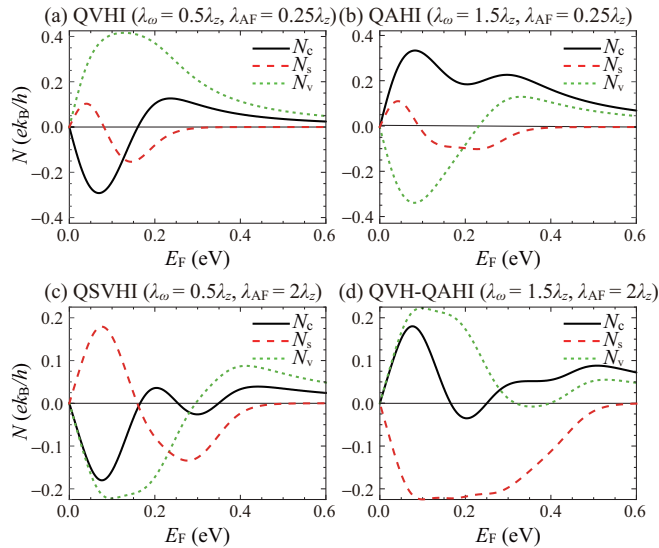
FIG. 6. Charge, spin, and valley Nernst conductivities as a function of E_F when both the external fields exist. (a) In the QVHI phase ($\lambda_\omega = 0.5\lambda_z$, $\lambda_{AF} = 0.25\lambda_z$); (b) in the QAHI phase ($\lambda_\omega = 1.5\lambda_z$, $\lambda_{AF} = 0.25\lambda_z$); (c) in the QSVHI phase ($\lambda_\omega = 0.5\lambda_z$, $\lambda_{AF} = 2\lambda_z$); (d) in the QVH-QAHI phase ($\lambda_\omega = 1.5\lambda_z$, $\lambda_{AF} = 2\lambda_z$).
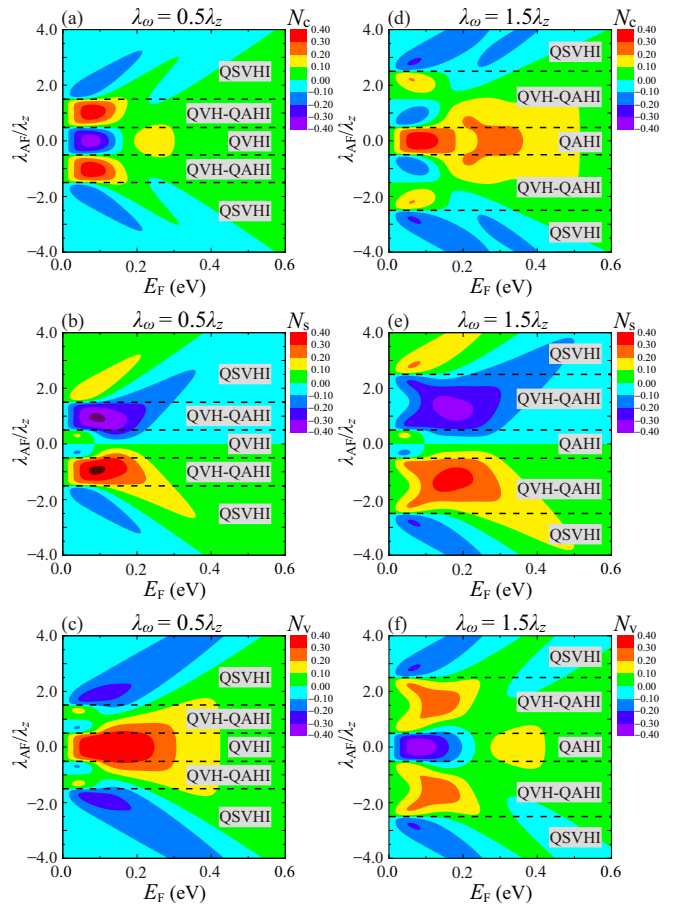
FIG. 7. (a) Charge N_c, (b) spin N_s, and (c) valley N_v Nernst conductivities as functions of E_F and λ_{AF} when $\lambda_\omega = 0.5\lambda_z$. (d) Charge N_c, (e) spin N_s, and (f) valley N_v Nernst conductivities as functions of E_F and λ_{AF} when $\lambda_\omega = 1.5\lambda_z$. Dashed lines represent phase boundaries.

i.e., by modulating E_F in the QVHI phase, the signs of N_c and N_s change, while the sign of N_v is always unchanged. In the QAHI phase, the sign changes of N_v and N_s occur, while the sign of N_c always remains unchanged. In the QSVHI phase, the signs of N_c, N_v, and N_s all change. However, in the QVH-QAHI phase, the changes of the signs of N_c and N_v become undetermined, which is related to the parameter selection of the external fields, but the only certainty is that the sign of N_s remains unchanged, which is a very obvious signature different from QVHI, QAHI, and QSVHI phases. We summarize the sign change of the Nernst conductivity in different topological phases in Table III. Therefore, tuning the Fermi level and detecting the sign changes of charge, spin, and valley Nernst conductivities can provide an executable method to distinguish abundant topological phases in epitaxial graphene.

V. TEMPERATURE DEPENDENCE OF THE ANOMALOUS NERNST EFFECT

We further calculate the effect of temperature on the anomalous Nernst conductivity. The temperature effect is

TABLE III. The relation between topological phase and sign change or unchange of the Nernst conductivity. Yes (No) represents the sign change (unchange) of the corresponding Nernst conductivity by modulating the Fermi level E_F.

Topological	Nernst conductivity		
phase	N_c	N_v	N_s
QVHI	Yes	No	Yes
QAHI	No	Yes	Yes
QSVHI	Yes	Yes	Yes
QVH-QAHI	Yes/No	Yes/No	No

shown in Fig. 8, where we plot the charge, spin, and valley Nernst conductivities versus E_F for different various topological phases and temperatures. The parameters of the external fields are chosen as exactly as those in Fig. 6. Since the anomalous Nernst conductivity is an odd function of E_F, we consider only the positive values of E_F. It is shown that the magnitudes of the valley Nernst conductivity in the QVHI phase, the charge Nernst conductivity in the QAHI phase, and the spin Nernst conductivity in the QVH-QAHI phase are enhanced significantly as the temperature increases, and the sign changes of charge, spin, and valley Nernst conductivities are robust against the temperature.

For showing the temperature dependence of the anomalous Nernst conductivity more clearly, we give some analytical results. At low temperatures, the Mott relation between spin-valley-dependent anomalous Nernst and Hall conductivity is [21]

$$N_{\eta,s_z} = \frac{\pi^2 k_B^2 T}{3e} \frac{d\sigma_{\eta,s_z}(E_F)}{dE_F}, \tag{7}$$

where

$$\sigma_{\eta,s_z} = \frac{e^2}{\hbar} \sum_n \int \frac{d\boldsymbol{k}}{(2\pi)^2} \Omega_{\eta,s_z}^n f_{\eta,s_z}^n(k) \tag{8}$$

is the spin-valley-dependent Hall conductivity. If $E_F > |\Delta_{\eta,s_z}|$, i.e., the Fermi level E_F lies in the conduction band, a simplified formula can be obtained from Eq. (8), that is,

$$\sigma_{\eta,s_z} = -\frac{e^2}{h} \frac{\eta \Delta_{\eta,s_z}}{4E_F}, \tag{9}$$

where $E_F = \sqrt{(\hbar v_F k_F)^2 + \Delta_{\eta,s_z}^2}$. Similar results can be obtained when the Fermi level E_F is in the valence band due to the symmetry. Substituting Eq. (9) into Eq. (7), an analytical expression for the spin-valley-dependent Nernst conductivity at low temperature can be derived, i.e.,

$$N_{\eta,s_z} = \frac{\pi^2}{12} \frac{ek_B^2 T}{h} \frac{\eta \Delta_{\eta,s_z}}{E_F^2}. \tag{10}$$

The Mott relation in Eq. (10) is derived from the traditional thermoelectric transport theory. Therefore it is necessary to verify its validity in our system. As shown in Fig. 9, we plot the spin-valley-dependent Nernst conductivities in different topological phases at $E_F = 0.5$ eV as a function of the environmental temperature T by using the Mott relation and numerical calculations. The solid line represents the result of numerical calculation, and the dashed line represents the result of the Mott relation. At low temperatures the results are in good agreement, which indicates that the traditional Mott relation is still suitable in the present situation.

However, it can be found that for the QVHI phase, the K (K') valley Nernst current increases (decreases) with the temperature, as shown in Fig. 9(a). Thus a valley electron
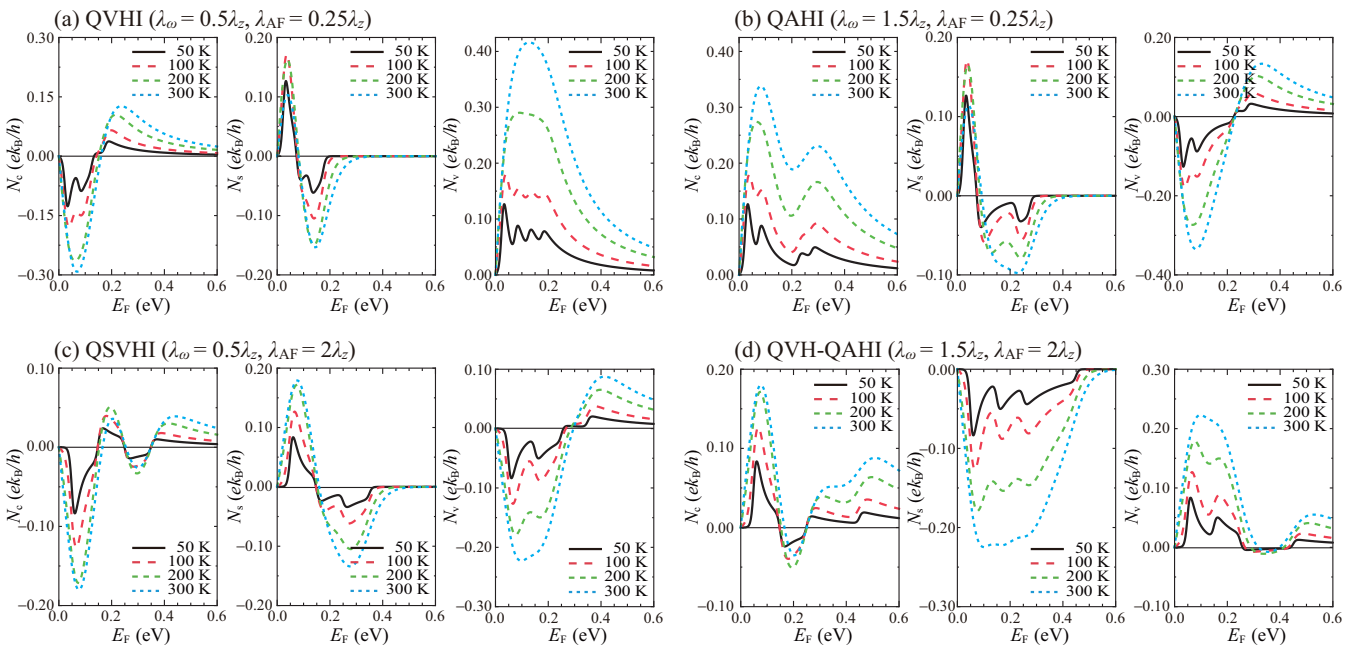
FIG. 8. Charge, spin, and valley Nernst conductivities vs E_F for various temperatures. The parameters of external fields correspond exactly to those in Fig. 6.
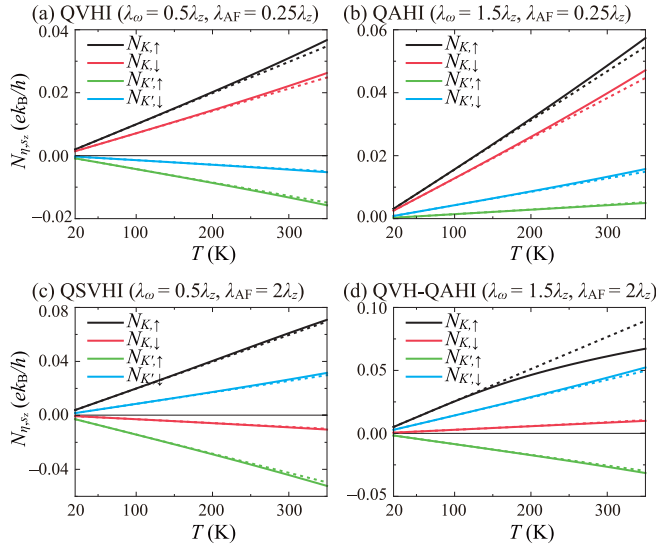
FIG. 9. Spin-valley-dependent Nernst conductivities vs T for different topological phases and fixed $E_F = 0.5\,\text{eV}$. The solid (dashed) line denotes the results of numerical (analytical) calculations.

beam splitter with larger current can be realized with increasing temperature. In Fig. 9(b), for the QAHI phase, all four components of the Nernst current increase with temperature. Therefore when the external field is fixed, in order to obtain a larger unidirectional Nernst current, it can be achieved by increasing the environmental temperature. For the QSVHI phase, the spin-valley-dependent Nernst currents $N_{K,\uparrow}$ and $N_{K',\downarrow}$ increase with increasing temperature, while $N_{K,\downarrow}$ and $N_{K',\uparrow}$ decrease with increasing temperature, as shown in Fig. 9(c). In the QVH-QAHI phase, three components of the Nernst current increase when the temperature raises, and the Nernst current with one valley and one spin decreases with the increase of temperature, as shown in Fig. 9(d). The change of spin-valley-dependent Nernst currents with increasing temperature in all topological phases is summarized in Table IV.

TABLE IV. The change of the spin-valley-dependent Nernst conductivities with increasing temperature in various topological phases. $\nearrow$ ($\searrow$) represents the spin-valley-dependent Nernst currents increase (decrease) with increasing temperature.

Topological phase	Chern numbers $[\mathcal{C}_c, \mathcal{C}_s, \mathcal{C}_v, \mathcal{C}_{sv}]$	Spin-valley Nernst conductivity			
		$N_{K,\uparrow}$	$N_{K,\downarrow}$	$N_{K',\uparrow}$	$N_{K',\downarrow}$
QVHI	$[0, 0, -2, 0]$	$\nearrow$	$\nearrow$	$\searrow$	$\searrow$
QAHI	$[-2, 0, 0, 0]$	$\nearrow$	$\nearrow$	$\nearrow$	$\nearrow$
	$[2, 0, 0, 0]$	$\searrow$	$\searrow$	$\searrow$	$\searrow$
QSVHI	$[0, 0, 0, -2]$	$\nearrow$	$\searrow$	$\searrow$	$\nearrow$
	$[0, 0, 0, 2]$	$\searrow$	$\nearrow$	$\nearrow$	$\searrow$
QVH-QAHI	$[-1, -1, -1, 1]$	$\nearrow$	$\nearrow$	$\nearrow$	$\searrow$
	$[-1, 1, -1, -1]$	$\nearrow$	$\nearrow$	$\searrow$	$\nearrow$
	$[1, -1, -1, -1]$	$\nearrow$	$\searrow$	$\searrow$	$\searrow$
	$[1, 1, -1, 1]$	$\searrow$	$\nearrow$	$\searrow$	$\searrow$

It can be concluded that in the QVHI phase, the spin-valley Nernst currents from the same valley have the same variation trend with increasing temperature. In the QAHI phase, the four components of the Nernst current all increase or decrease with increasing temperature. In the QSVHI phase, the Nernst currents from different valleys and different spins have the same variation trend with increasing temperature. In the QVH-QAHI phase, the three components of the Nernst current have the same variation trend with increasing temperature, while the Nernst current with one valley and one spin is the opposite variation trend with increasing temperature. The spin- and valley-dependent Nernst conductivity can be measured by multiterminal inverse spin and valley Hall setups in experiments [44]. Through these numerical calculations and analytical expressions, it is found that adjusting the sample temperature to measure the variation trend of the spin- and valley-dependent Nernst currents can characterize whether the topological phase transition occurs in epitaxial graphene, providing a way to distinguish topological phases and another degree of freedom to modulate Nernst currents experimentally.

It should be noted that in experimental measurements, electron-hole puddles always exist in real graphene devices due to impurity correlations in the substrate [45]. When the Fermi level is tuned to the vicinity of the charge neutrality point, the Nernst conductivity is affected and the Mott relation is not applicable because of the presence of electron and hole puddles [46–48]. In fact, an interesting work on twisted bilayer graphene showed that by introducing the electron-hole puddle parameter through the density of states, the Seebeck coefficient is affected at different temperatures, and the violation of the Mott relation is also observed in the experiment [49]. Therefore the electron-hole puddles could lead to deviations between the theoretical calculations and experimental results near the Dirac point. Fortunately, in our work the gap in most topological phases is larger, and the Fermi level is away from the Dirac cone so that the influence of the electron-hole puddles in most topological phases is assumed to be negligible. In addition, the tendency of the Nernst conductivities with the Fermi level or temperature also is maintained when the Fermi level is tuned away from this electron-hole puddle regime. The behavior of the Nernst conductivities and the correspondence between topological phases would be qualitatively correct.

VI. CONCLUSIONS

In summary, we have systematically investigated the anomalous Nernst effect based on the Berry curvature in epitaxial graphene under the coaction of off-resonant light and antiferromagnetic fields and propose two new methods to differentiate various topological phases. The results have shown that when either the light field or antiferromagnetic field is zero, the spin Nernst current is zero. When the light field is zero, the charge Nernst current is zero. Due to the existence of the substrate potential, a thermally induced pure valley current can be demonstrated, and its magnitude and sign can be controlled by tuning the antiferromagnetic exchange field. At room temperature, single-spin and single-valley Nernst currents can be collected in the QVH-QAHI phase. In the QAHI phase, a unidirectional Nernst current can be achieved.

The abundant topological phases in epitaxial graphene can be distinguished by detecting the sign change of the charge, spin, and valley Nernst conductivities by tuning the Fermi level. In addition, we have investigated the temperature dependence of Nernst conductivity, and it is shown that the sign change of the Nernst conductivity is robust against a weak temperature. The magnitudes of the valley Nernst conductivity in the QVHI phase, the charge Nernst conductivity in the QAHI phase, and the spin Nernst conductivity in the QVH-QAHI phase are enhanced significantly as the temperature increases. The Nernst conductivity can be related to the Hall conductivity via the semiclassical Mott relation, and we have given an analytical expression for the spin-valley-dependent Nernst conductivity at low temperature. In different topological phases, the spin-valley-dependent Nernst currents have different trends with increasing temperature. By probing the spin- and valley-dependent Nernst current variation trend by adjusting the sample temperature, we can also characterize whether topological phase transitions occur in epitaxial graphene. These findings are expected to promote applications in spin and valley caloritronics.

[1] K. S. Novoselov, A. K. Geim, S. V. Morozov, D. Jiang, Y. Zhang, S. V. Dubonos, I. V. Grigorieva, and A. A. Firsov, Science **306**, 666 (2004).

[2] A. H. Castro Neto, F. Guinea, N. M. R. Peres, K. S. Novoselov, and A. K. Geim, Rev. Mod. Phys. **81**, 109 (2009).

[3] C. L. Kane and E. J. Mele, Phys. Rev. Lett. **95**, 226801 (2005).

[4] S. Das Sarma, S. Adam, E. H. Hwang, and E. Rossi, Rev. Mod. Phys. **83**, 407 (2011).

[5] R. C. Andrew, R. E. Mapasha, A. M. Ukpong, and N. Chetty, Phys. Rev. B **85**, 125428 (2012).

[6] D. Xiao, W. Yao, and Q. Niu, Phys. Rev. Lett. **99**, 236809 (2007).

[7] A. Avsar, H. Ochoa, F. Guinea, B. Özyilmaz, B. J. van Wees, and I. J. Vera-Marun, Rev. Mod. Phys. **92**, 021003 (2020).

[8] S. V. Morozov, K. S. Novoselov, M. I. Katsnelson, F. Schedin, L. A. Ponomarenko, D. Jiang, and A. K. Geim, Phys. Rev. Lett. **97**, 016801 (2006).

[9] A. F. Morpurgo and F. Guinea, Phys. Rev. Lett. **97**, 196804 (2006).

[10] S. A. Vitale, D. Nezich, J. O. Varghese, P. Kim, N. Gedik, P. Jarillo-Herrero, D. Xiao, and M. Rothschild, Small **14**, 1801483 (2018).

[11] D. Xiao, M.-C. Chang, and Q. Niu, Rev. Mod. Phys. **82**, 1959 (2010).

[12] X. Zhou, Y. Xu, and G. Jin, Phys. Rev. B **92**, 235436 (2015).

[13] Y. Xu, J. Ma, and G. Jin, Phys. Rev. B **104**, 045416 (2021).

[14] M. Ezawa, Eur. Phys. J. B **85**, 363 (2012).

[15] M. Ezawa, Phys. Rev. B **86**, 161407(R) (2012).

[16] C. Zhang, S. Tewari, and S. Das Sarma, Phys. Rev. B **79**, 245424 (2009).

[17] M. Tahir and P. Vasilopoulos, Phys. Rev. B **91**, 115311 (2015).

[18] Y. Xu, X. Zhou, and G. Jin, Appl. Phys. Lett. **108**, 203104 (2016).

[19] G. Sharma, Phys. Rev. B **98**, 075416 (2018).

[20] Y. Xu and X. Li, Europhys. Lett. **132**, 47001 (2020).

[21] D. Xiao, Y. Yao, Z. Fang, and Q. Niu, Phys. Rev. Lett. **97**, 026603 (2006).

[22] X. Li, T. Cao, Q. Niu, J. Shi, and J. Feng, Proc. Natl. Acad. Sci. USA **110**, 3738 (2013).

[23] S. Y. Zhou, G.-H. Gweon, A. V. Fedorov, P. N. First, W. A. de Heer, D.-H. Lee, F. Guinea, A. H. Castro Neto, and A. Lanzara, Nat. Mater. **6**, 770 (2007).

[24] E. Rotenberg, A. Bostwick, T. Ohta, J. L. McChesney, T. Seyller, and K. Horn, Nat. Mater. **7**, 258 (2008).

[25] M. Ezawa, Phys. Rev. Lett. **110**, 026603 (2013).

[26] T. Kitagawa, T. Oka, A. Brataas, L. Fu, and E. Demler, Phys. Rev. B **84**, 235108 (2011).

[27] A. Roberts, D. Cormode, C. Reynolds, T. Newhouse-Illige, B. J. LeRoy, and A. S. Sandhu, Appl. Phys. Lett. **99**, 051912 (2011).

[28] X. Zhai, Y.-T. Wang, R. Wen, S.-X. Wang, Y. Tian, X. Zhou, W. Chen, and Z. Yang, Phys. Rev. B **97**, 085410 (2018).

[29] W.-T. Lu and Q.-F. Sun, Phys. Rev. B **108**, 075422 (2023).

[30] M. Ezawa, Phys. Rev. B **87**, 155415 (2013).

[31] P. Högl, T. Frank, K. Zollner, D. Kochan, M. Gmitra, and J. Fabian, Phys. Rev. Lett. **124**, 136403 (2020).

[32] K. Zollner and J. Fabian, Phys. Rev. B **106**, 035137 (2022).

[33] J. C. Leutenantsmeyer, A. A. Kaverzin, M. Wojtaszek, and B. J. van Wees, 2D Mater. **4**, 014001 (2017).

[34] P. Gargiani, R. Cuadrado, H. B. Vasili, M. Pruneda, and M. Valvidares, Nat. Commun. **8**, 699 (2017).

[35] L. Tamang and T. Biswas, Phys. Rev. B **107**, 085408 (2023).

[36] Y.-L. Wu, G.-H. Zhu, and X.-Q. Yu, Phys. Rev. B **104**, 195427 (2021).

[37] Y. You, H. Lam, C. Wan, C. Wan, W. Zhu, L. Han, H. Bai, Y. Zhou, L. Qiao, T. Chen, F. Pan, J. Liu, and C. Song, Phys. Rev. Appl. **18**, 024007 (2022).

[38] K. Gadge, S. Tewari, and G. Sharma, Phys. Rev. B **105**, 235420 (2022).

[39] H. Sun, S.-S. Li, W.-X. Ji, and C.-W. Zhang, Phys. Rev. B **105**, 195112 (2022).

[40] Q.-Q. Zhang, Q. Li, X.-T. An, and J.-J. Liu, Phys. Rev. B **105**, 205436 (2022).

[41] K. Ando and E. Saitoh, Nat. Commun. **3**, 629 (2012).

[42] Y. Jiang, T. Low, K. Chang, M. I. Katsnelson, and F. Guinea, Phys. Rev. Lett. **110**, 046601 (2013).

[43] M. Yamamoto, Y. Shimazaki, I. V. Borzenets, and S. Tarucha, J. Phys. Soc. Jpn. **84**, 121006 (2015).

[44] X. Zhai and Y. M. Blanter, Phys. Rev. B **102**, 075407 (2020).

[45] J. Martin, N. Akerman, G. Ulbricht, T. Lohmann, J. H. Smet, K. Von Klitzing, and A. Yacoby, Nat. Phys. **4**, 144 (2008).

[46] X.-Z. Yan and C. S. Ting, Phys. Rev. B **81**, 155457 (2010).

[47] Y. M. Zuev, W. Chang, and P. Kim, Phys. Rev. Lett. **102**, 096807 (2009).

[48] Q. Feng, T. Zhu, Y. Jian, W. Yuan, H. Peng, J. Zhong, J. Duan, and M. Zebarjadi, J. Phys. D: Appl. Phys. **55**, 455303 (2022).

[49] P. S. Mahapatra, K. Sarkar, H. R. Krishnamurthy, S. Mukerjee, and A. Ghosh, Nano Lett. **17**, 6822 (2017).